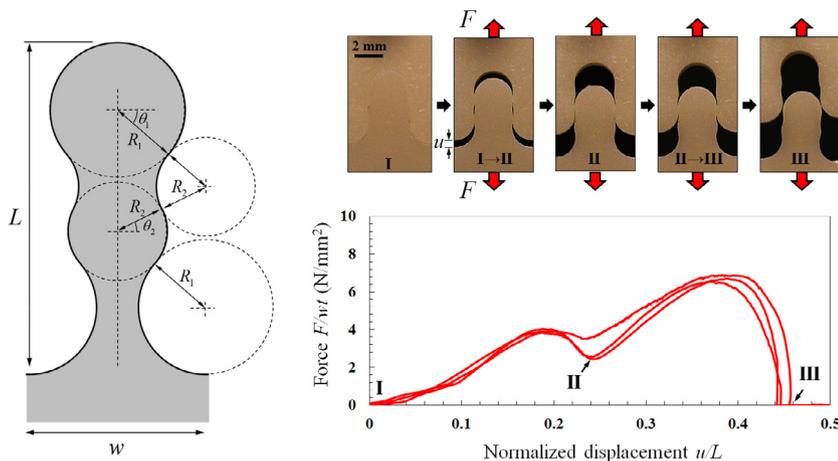# Design, 3D printing and testing of architectured materials with bistable interlocks

Mohammad Mirkhalaf, Francois Barthelat *

Department of Mechanical Engineering, McGill University, 817 Sherbrooke Street West, Montreal, QC H3A 2K6, Canada

GRAPHICAL ABSTRACT

ARTICLE INFO

ABSTRACT

Mechanisms associated with geometric interlocking are critical in engineering materials such as adhesives, metals or composites, and also in natural materials such as diatoms or mollusk shells. In this work we developed a new type of sutured material based on jigsaw-like morphologies which can be programmed to geometrically lock into two distinct stable positions. Using 3D printing and design exploration, we show that the mechanical response of these bistable materials can be tailored by fine tuning of the architecture of the tabs. The system can be cycled between the two equilibrium positions without apparent damage accumulation. We also show that the second equilibrium position can be made more stable than the first, effectively providing a geometric hardening mechanism to delay localization and spread nonlinear deformations over large volumes of material. The resulting materials are up to 10 times tougher than the polymer they are made of and they offer attractive properties such as large and reversible deformations, damage tolerance and re-manufacturability, offering promising perspectives in the development of new architectured materials.

* Corresponding author.
  E-mail address: francois.barthelat@mcgill.ca (F. Barthelat).

1. Introduction

Geometric interlocking plays a critical role in the cohesion and adhesion of materials and structures, for example in adhesive science and engineering [1], in friction and tribology [2], in the plasticity and creep of ductile metals [3], or in fiber reinforced composites [4]. Recently, architectured materials based on the topologically interlocking of building blocks have shown unusual and attractive combinations of properties [5–12]. Geometric interlocking is also present in nature, for example in sutures with intricate geometries that ensure the strong and often compliant joining of structural elements in ammonite shells, turtle shells or in diatoms [13–16]. Interface mechanisms are also critical in hard biological materials such as bone or nacre, where they dissipate energy and generate toughness in otherwise brittle minerals [17,18]. In this study, we introduce a new type of sutured material which combines the concepts of geometric interlocking, bio-inspiration and architecture. We also implement and explore multi-stability in these sutures, with implications which are similar to phase transforming cellular materials [19–21], multi-stable origami [22–25], kirigami structures with voids of switchable and multistable geometry [26,27], or bilayer orthotropic materials [28]. However, unlike the previous multi-stable materials which are based on reversible elastic deformations between stable configurations, our material involves sliding and interlocking between two stable states.

2. Design of bistable interlocked materials (BIM)

The new bistable interlocked materials (BIMs) are based on controlled separation and pullout of sutures with well controlled geometries. The design of the suture is based on jigsaw-like contours built from a series of arcs of circle with radii R_1 and R_2, which are blended tangentially at locations defined by angles θ_1 and θ_2 (Fig. 1(a)). Round features were chosen for their simplicity, and also because they reduce stress concentrations in the solid. The pattern is symmetric about the axis of the tab, and follows a $\pm 180°$ rotational symmetry (Fig. 1(a)). This profile can be used as a "unit cell" in long two-dimensional suture lines with a periodic pattern. To simplify the discussion and to emphasize the effect of geometry, we did not consider or use any adhesive at the suture line, so that only mechanical interlocking, contact mechanics and friction govern the interactions of the tabs. The mechanisms of interest associated with this particular suture geometry are shown on Fig. 1(b). The initial configuration is at rest, and provides a first stable position for the system (stage I). When tensile stresses are applied across the suture line, the tab is pulled out of its initial position, which is resisted by geometric interference, contact stresses and friction acting at two pairs of contact points (stage I→II). Further pullout brings the end of the tabs to a second cavity-like geometry which locks the system in a second stable position (stage II). From that position, compression may be applied on the tabs to bring the system back to the first stable position (II→I). Alternately, further tension may be applied to pull the tab further until complete pullout (III).

The mechanical response of the system across its different states can be programmed through a small set of geometric parameters. For example, higher locking angles increase geometric interference and increase the force required for pullout. The radius R_1 can also be made larger than R_2 to increase the force required for complete pullout, an interesting feature which we further developed in this work. Since all the mechanisms rely on elasticity of the bulk material and friction, there is no particular length scale associated with the mechanisms and therefore the non-dimensional R_1/R_2 was used. In addition, examination of the geometry reveals that the four parameters (R_1, R_2, θ_1, θ_2) are not independent form one another. In particular, the angle θ_2 can be written:

$$\theta_2 = \cos^{-1}\left[\frac{1}{2}\left(\frac{R_1}{R_2} + 1\right)\cos\theta_1\right]. \tag{1}$$

The non-dimensional geometry of the tab is therefore fully defined by the two independent parameters R_1/R_2 and θ_1. Other dimensions of interest in the structure are the length L and the width w of the tab, given by:

$$L = 2\left[R_1(1 + \sin\theta_1) + R_2(\sin\theta_1 + \sin\theta_2)\right] \tag{2}$$

$$w = 2(R_1 + R_2)\cos\theta_1. \tag{3}$$

There are geometric constraints on R_1/R_2 and θ_1 which restrict the range of possible designs for this structure. Eq. (1) has a solution only if:

$$\frac{R_1}{R_2} \leq \frac{2}{\cos\theta_1} - 1. \tag{4}$$

In addition, the contour of the suture cannot intersect itself, a physical condition which can be written:

$$\frac{1 - \cos\theta_1}{\cos\theta_1} < \frac{R_1}{R_2} < \frac{\cos\theta_1}{1 - \cos\theta_1}. \tag{5}$$

Eqs. (4) and (5) define the boundaries of an admissible domain in the design space (R_1/R_2, θ_1), which is shown on Fig. 1(c). Within this domain, these parameters can be tuned to generate a wide range of geometries as shown on Fig. 1(d). We expect that the cases where $R_1/R_2 < 1$ will only provide loose and unstable second equilibrium positions, and therefore only the cases $R_1/R_2 \geq 1$ are mechanically and functionally relevant. We also expect that cases where the interlocking angle θ_1 and/or ratio R_1/R_2 are too high may lead to excessive stresses and fracture of the tabs, an undesired failure mode for the suture.

3. 3D printing and testing of individual bistable interlocked tabs

We explored the design and performance of this interlocked suture using 3D printed samples with different combinations of interlocking angles ($\theta_1 = 5°$, $15°$, $25°$, $35°$) and radii $R_1/R_2 = 1$, 1.03, 1.05, 1.06 (all samples had a thickness $t = 2$ mm). We used a high-resolution 3D printer (Micro HiRes Machine, EnvisionTech) which is based on the Digital Light Processing (DLP) technology [29,30]. This technique enables the 3D printing of pore-free, homogeneous and mechanically isotropic components. The high spatial-resolution of that printer ($\sim$80 µm) allowed for high morphological fidelity, and produced materials with smooth surfaces which was critical for consistent friction coefficient and to minimize stress concentrations. The base material was a UV-curable acrylonitrile butadiene styrene (ABS, EnvisionTech Perfactory, MI, US). ABS is a relatively stiff and strong polymer ($E = 1.7 \pm 0.2$ GPa flexural strength $= 118 \pm 12$ MPa, measured experimentally with flexural tests) but it is also relatively brittle, with a flexural strain at failure of 0.112 ± 0.18. The two solid parts that make the interlocked tab were first 3D printed individually, and then assembled by sliding them together along the out-of-plane direction (Fig. 2(a)). The assembly was smooth and involved a minimal amount of force along the out-of-plane direction. Detailed microscopy of the individual parts with different combinations of θ_1 and R_1/R_2 revealed that the gap at the interfaces after assembly was about 8 µm. This gap was small enough to assume that the tabs were initially in contact for the purpose of the analysis, but also large enough to ensure that the assembled solid tabs were free of stresses before testing. The total width of sample was about six times the width of the individual tab to minimize in-plane bending
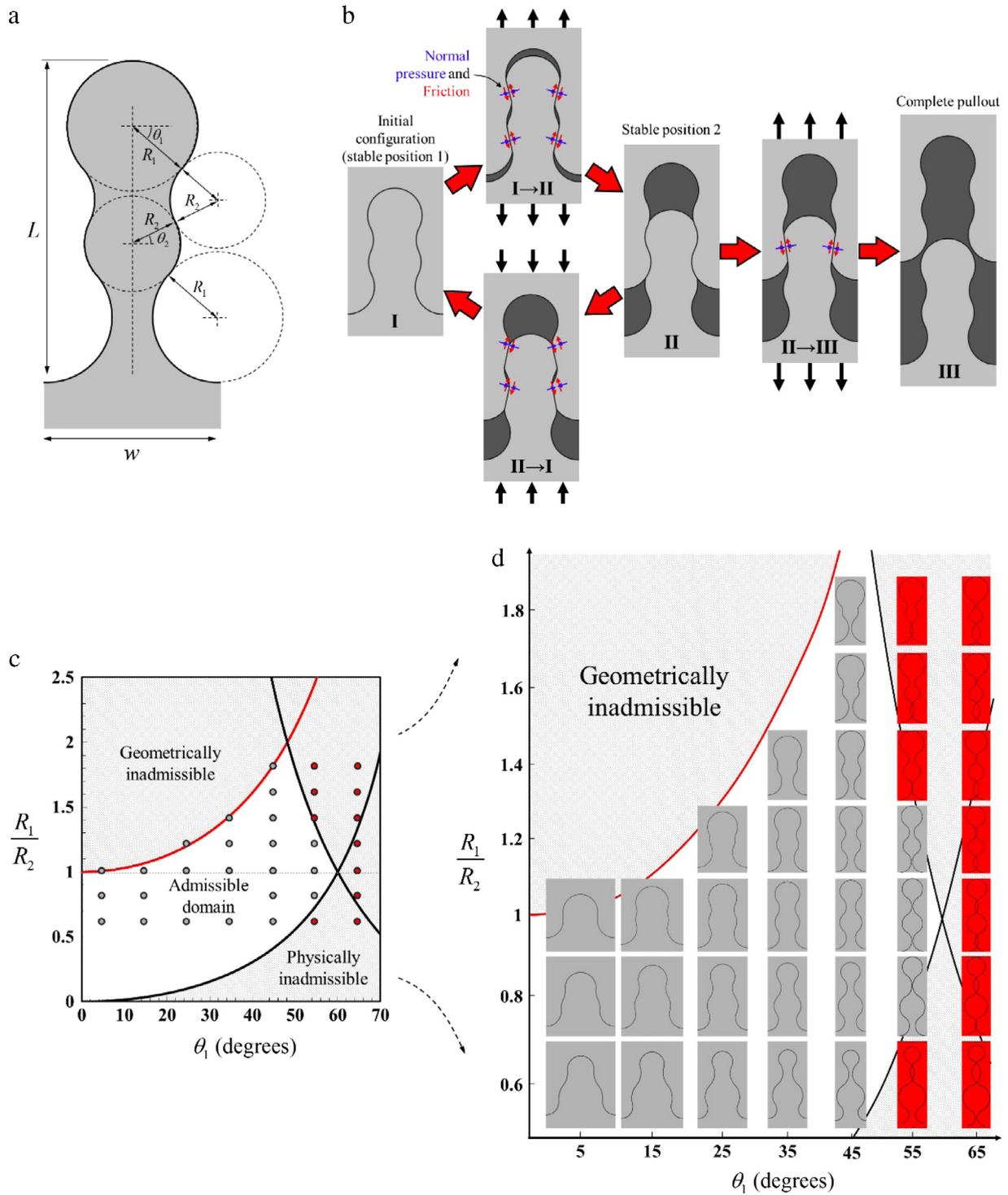
a

b

c

d

Fig. 1. Overview of the design of bistable interlocked tabs; (a) The profile of the tab consists of arcs of circles or radii R_1 and R_2 which blend according to angle θ_1. Angle θ_2 is dependent on R_1, R_2 and θ_1; (b) Mechanisms of pull and push. The system can be switched between the two stable positions I and II, or completely pulled out (III). Normal pressure, friction and contact mechanics govern the interactions of the tabs; (c) Design space for the independent parameters R_1/R_2 and θ_1, showing the domains which are inadmissible and admissible; (d) Examples showing how tuning R_1/R_2 and θ_1 within the admissible domain can leads to a wide range of geometries.

and deformation modes which are not representative of a long suture line (we verified experimentally that the total width of the sample was sufficiently large to have no effect on the mechanical response of the individual tabs). Tensile tests were performed on the tabs in quasi-static conditions (displacement rate = 5 μm/s) using a miniature loading machine (Ernest F Fullam, Inc., Latham, NY, USA). Three samples were tested for each configuration. Fig. 2(a) shows a set of typical tensile responses, where we use

F/wt for the traction and u/L for the pullout displacement in order to get a measure of the effective traction and deformation which would be obtained for a periodic suture. Initially the pullout traction increased, the pulling out of the tab being resisted by normal and frictional stresses at two pairs of contact points (stage I→II). The traction reached a first peak, then decreased when the tab approached its second stable position characterized by a local minimum on the curve (stage II). At this equilibrium position the

traction was zero for $R_1/R_2 = 1$, because the interlocking features fitted with no stresses in the solid parts. Further pulling of the tab dislodged the tab further into stage II→III, a process governed by the same contact and friction mechanisms as stage I→II. However, in stage II→III the pullout traction was transmitted through only one pair of contact points (Fig. 1(b)). For the case $R_1/R_2 = 1$, the parameters of the individual contact regions were identical in stage I→II and II→III, and as a result the pull traction at the second peak was only half of the traction at the first peak. For $R_1/R_2 = 1$ the system is therefore weaker in tension once the second position is reached, which is not advantageous in terms of overall stability. It is however possible to increase the second peak traction by adjusting the geometry of the tabs. Fig. 2(a) shows another traction–displacement curve for a tab with $R_1/R_2 = 1.05$ and $\theta_1 = 15°$. While this small increase in R_1/R_2 only slightly increased the first peak traction, it greatly increased the second peak. At the second stable position the end of the tab of radius R_1 must fit within a smaller cavity of radius $R_2 < R_1$. As result of this geometric interference and stronger interlocking, a higher traction was required to dislodge the system from that position and for complete pullout. This feature can be particularly useful to improve the stability of materials made of multiple suture lines, in a way similar to the way strain hardening delays localization and necking in ductile metals. Fig. 2(b) shows a typical result from a cyclic tests on a sample with $R_1/R_2 = 1.05$ and $\theta_1 = 15°$, where the system was cycled several times between positions I and II. The mechanical response of the tab is identical over multiple cycles, showing that repeatedly bringing the system between position I and position II does not degrade its performance. This result suggests that there is no permanent damage in the system, which is entirely governed by elastic deformations of the tabs, contact mechanics and friction. A more detailed stress analysis on the tab involves the solution from the frictional sliding contact between two disks. In this solution the interference δ is given by [31]:

$$\delta = \frac{a^2}{4R^*}\left[2\ln\left(\frac{8R^*}{a}\right) - 1\right] \tag{6}$$

where $\frac{1}{R^*} = \frac{1}{R_1} + \frac{1}{R_2}$ gives the reduced radius R^*, and a is the half width of the contact area which in plane stress condition is given by:

$$a^2 = \frac{8PR^*}{\pi tE}. \tag{7}$$

In Eq. (7) P is the contact force, t is the thickness of the tabs and E is the elastic modulus of the material. Meanwhile, the maximum contact pressure is given by:

$$p_0 = \frac{2P}{\pi ta}. \tag{8}$$

During the transition from the first to the second stable configuration, the maximum contact force and pressure will occur at the maximum interference, which is given by:

$$\delta_{\max} = (R_1 + R_2)(1 - \cos\theta_1). \tag{9}$$

Eqs. (6) through (9) can be combined and solved to compute the maximum contact pressure p_0 as a function of the maximum interference $\delta_{\max}$. We measured the modulus E and 0.2% offset yield strength of ABS ($E = 1.7 \pm 0.2$ GPa and $\sigma_y = 109.8 \pm 8.7$ MPa) using a three-point bending configuration. For the case $\theta_1 = 15°$, $R_1 = 1.05$ mm, and $R_2 = 1$ mm (Fig. 2(b)), we found a maximum pressure $p_0 = 124.5$ MPa. This maximum pressure was then used in a sliding contact model that includes friction. For this purpose we measured a friction coefficient of $f = 0.35$ between two flat surfaces of our 3D printed ABS (following ASTM D1894 [32]). To model yielding from frictional contact we used the model developed by Johnson and Jefferiss [31], which predicts an onset of yielding at a maximum contact pressure of $(p_0)_y = 0.8\sqrt{3}\sigma_y = 152.2$ MPa for a friction $f = 0.35$ (using the Von-Mises yield criterion). The model therefore predicts that no plastic deformations occur in the tabs with this set of geometry and material. We used 3D printing and tensile testing to explore how different combinations of θ_1 and R_1/R_2 could control the mechanical properties of the system. Fig. 2(c) shows how higher θ_1 and R_1/R_2 both increase the strength of the interlocked tab. However, we also found that beyond a threshold, the tabs fractured from excessive contact stresses (Fig. 2(c)), a detrimental failure mode which ruins the functionality of the suture. As discussed above, it is advantageous for the second peak to be higher than the first peak for mechanical stability. For the purpose of design and optimization it is convenient to define a peak ratio $\xi = F_2/F_1$ where F_1 and F_2 are the force at the first and the second peak. Fig. 2(d) shows that increasing $R_1/R_2 = 1$ to higher values increases the ratio ξ from 0.5 to almost 2.

4. Bistable interlocked materials (BIMs)

The attractive mechanical behavior of individual interlocked sutures can be duplicated over large volumes of materials, provided that an adequate hardening mechanism is programmed in the material [6]. Here we fabricated materials containing five parallel bistable interfaces spaced by a distance of 10 mm (Fig. 3(a), $t = 3$ mm). The parameters we used were $R_1/R_2 = 1.05$ and $\theta_1 = 15°$, which produced a good combination of high strength and high peak ratio ξ. The six parts of the sample were printed individually and then assembled manually. At rest, the interfaces were almost invisible. The samples were tested in tension at a displacement rate of 5 μm/s, and typical results are shown on Fig. 3(b), (c). In the first phase of the tensile test, all the sutures opened simultaneously (Point B and snapshot B on Fig. 3(b), (c)). As each suture progressed in the I→II transition, one of the sutures eventually reached position II, which was accompanied by a drop in stress (point C). This particular suture was however stable and did not open further, because the traction required for complete pullout (II→III) was larger than the traction needed to transform other sutures in the material to their second stable position (I→II). The benefit of this mechanism is that all the sutures could reach their second stable position (Fig. 3), spreading large deformations throughout the entire sample. The transformation of each of the interfaces was accompanied by sudden drops in stress, but the transition from I to II for all the sutures in the material after the first one transforms was not accompanied with any major increase or decrease of stress. This type of "plateau regime" in the stress–strain curve is typical of phase transforming materials activated by stresses. [20,33]. The stiffness of the BIMs was 61 ± 7.6 MPa, its tensile strength 6.5 ± 0.8 MPa, its strain at failure 0.4 ± 0.03, and its energy absorption 1634 ± 178 kJ/m^3 ($N = 3$ samples). For comparison, the mechanical properties of the as-printed ABS material were measured using three-point bending ($N = 3$): The modulus for this material is $E = 1.7 \pm 0.2$ GPa, strength $\sigma_S = 118 \pm 12$ MPa, strain at failure $= 0.112 \pm 0.18$ and energy absorption $U_S = 7560 \pm 90$ kJ/m^3. Compared to pure ABS, the ABS bistable interlocked material is therefore is ~30 times less stiff, and ~20 times weaker, and 4.5 time less energy absorbent in tension but it shows ~4 times more strain at failure. However, for a relatively brittle material such as the ABS used in this study (the failure of plain ABS was catastrophic), the area under the stress–strain curve does not represent the actual energy dissipation within the material because the stored energy is released by dynamic effects or transferred to the connective components upon failure [34].

a Monotonic pullout
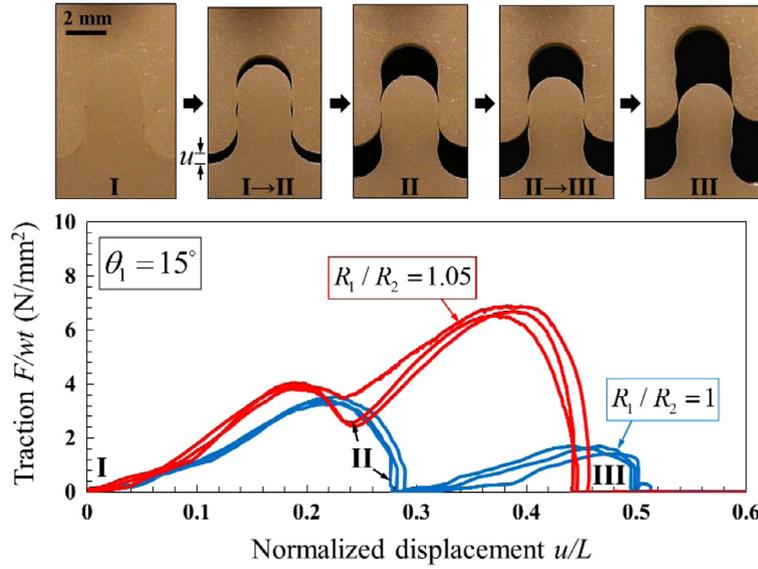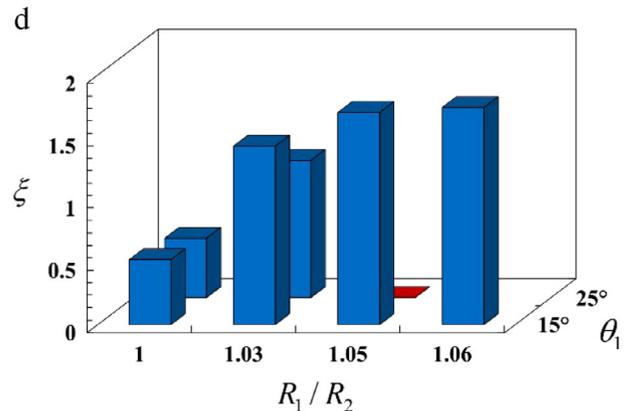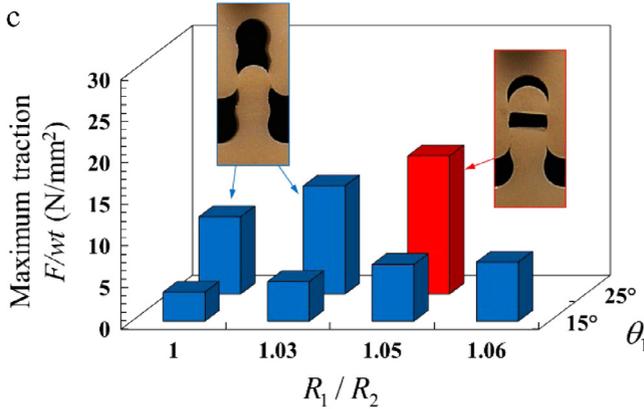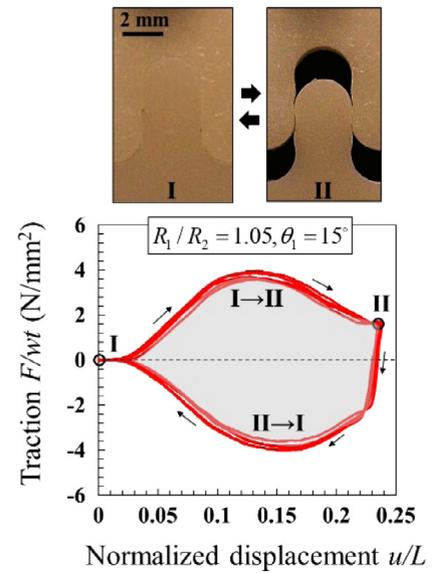

b Cyclic loading

Fig. 2. Tensile behavior of individual bistable interlocked tabs; (a) Typical sequence of a pullout test and traction–displacement curves of the bistable interlocked tab. The shape of the pullout curve can be tuned with R_1/R_2 and θ_1. In particular, the second peak can be made stronger by increasing R_1/R_2. (b) Cyclic tests that show that the system can be brought between positions I and II an indefinite number of times and without any apparent accumulation of damage. (c) Effect of R_1/R_2 and θ_1 on the maximum pullout traction. Higher R_1/R_2 and θ_1 lead to stronger tabs, but may fracture the solid material. (d) Effect of R_1/R_2 and θ_1 on the peak ratio ξ showing that one can achieve $\xi > 1$ with high R_1/R_2.

5. Crack propagation and toughness

The tensile tests demonstrated that the bistable interlocking can spread deformation and frictional energy dissipation throughout an otherwise brittle material if the design parameters are carefully selected. In this section we explore the capability of the material to resist crack propagation and to redistribute stresses over large volumes around defects. We build a larger plate made of individual building blocks containing interlocking features with $\theta_1 = 15°$ and $R_1/R_2 = 1.05$ (Fig. 4(a)). The blocks were assembled in a staggered fashion to form large plates containing a long initial notch simulating an initial crack (Fig. 4(a)). These fracture samples were composed of 48 building blocks arranged in 4×12 arrays with overall dimensions of ∼56 mm by ∼56 mm (thickness = 3 mm), with an initial notch depth of 14 mm. The upper and lower ends of the plate were clamped in a dual column loading stage (Admet, model eXpert 5000, MA US) and stretched at a constant displacement rate of 5 μm/s. Fig. 4(b) shows three force–deflection curves for this test, and Fig. 4(c) shows representative snapshots of the sample taken during testing. The force initially increased linearly as the blocks sled on one another. At early stages of the

loading, a small drop in force was observed as a result of the transformation of the interlocked tabs just ahead of the notch (Fig. 4 point B). This nonlinear deformation then spread over a triangular region ahead of the notch, relieving the high stresses, dissipating energy through friction and contributing to overall toughness through a process zone-like mechanism [35,36]. As the crack propagated, several drops in force were observed. However, the material still resisted deformation and several interfaces ahead of the crack transformed (Fig. 4, points C, D, E) before complete fracture of the material, which occurred by pullout of the tabs (Fig. 4, point F). The fracture toughness, obtained by dividing the area under the force–deflection curve to the area of the initial un-cracked ligament, was 3500 ± 386.8 J m^{-2} ($N = 3$) for the sutured material. For comparison, we measured a toughness of 300 ± 28.6 J m^{-2} for plain ABS, using a 3-point-bending fracture test configuration [37]. The fracture toughness of the bistable interlocked material is therefore more than 10 times higher than the plain ABS, resulted from a process-zone type toughening mechanisms associated with controlled pullout, spreading of nonlinear deformation and energy dissipations. These mechanisms are similar to the main fracture mechanisms in high performance biological materials [36,38,39].
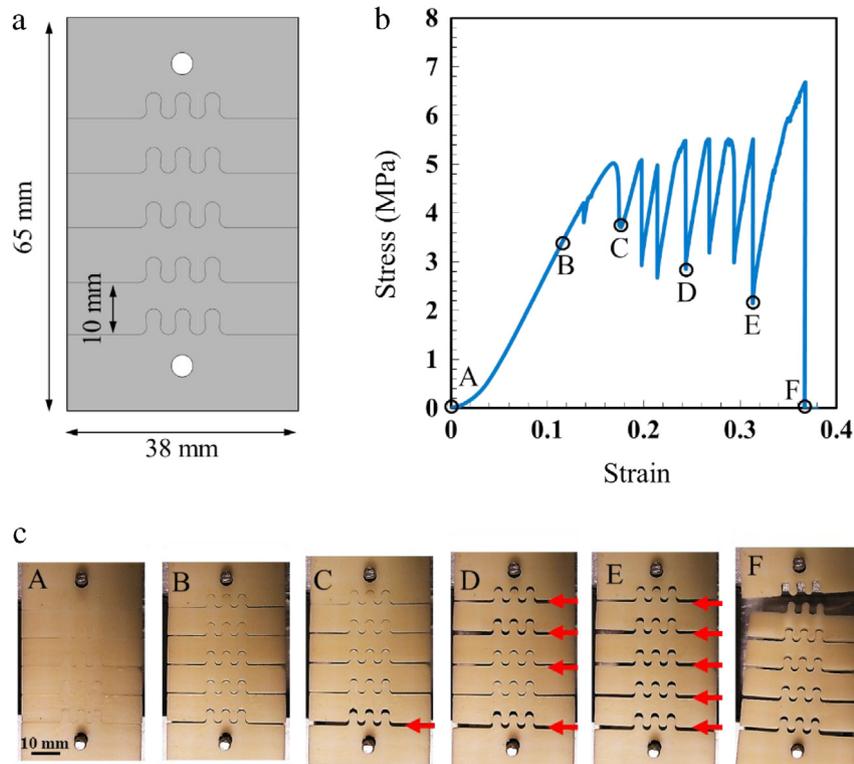
Fig. 3. A bistable interlocked material (BIM); (a) Geometry of the tensile test sample with multiple interlocked sutures; (b) A typical tensile stress–strain curve (here with $\theta_1 = 15°$ and $R_1/R_2 = 1.05$) showing a plateau-like region corresponding to the transformation of the sutures. (c) In-situ images showing different stages of loading and progressive transformation of tabs to their second stable configuration. All the potential sites have transitioned to the second stable position (stage E) prior to complete failure (stage F).
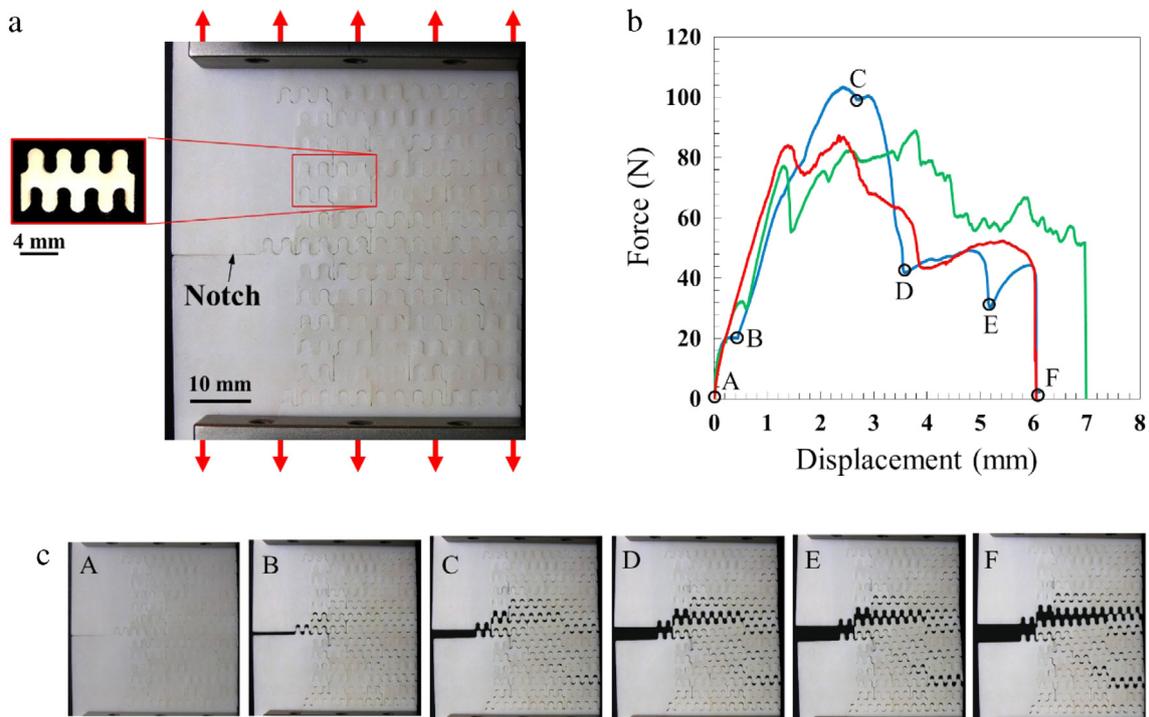

Fig. 4. Fracture behavior of the BIMs; (a) Individual block and assembled plate; (b) Force–deflection curves for three different samples. The bell shape of the curves is characteristic of tough materials; (c) In-situ images showing the formation of a triangular process-zone in front of the notch, followed by progressive fracture.

6. Summary

Mechanisms associated with geometric interlocking and sutures are prevalent in natural structural materials, and have a strong potential in engineering which has yet to be fully exploited. Here we introduce a novel bistable suture which can be cycled between two equilibrium states an indefinite number of times. The geometry of the suture can also be finely tuned to generate

a hardening mechanism based at large deformations, which can be used to delocalize the strains and improve the fracture toughness of a brittle material such as ABS. Compared to plain ABS, our bistable interlocked materials (BIMs) show an improvement of toughness and strain at failure by up to 10 folds, at the expense of 10–30 fold decrease in strength and modulus (for comparison, bistable cellular materials are two to four orders of magnitude softer than the solid materials of which they are made [20]). This strategy can be used to create tailored sutures with other types of materials, interfaces, and different length scales. The positions of stability can be pre-programmed with the geometry of the tabs, while strength and energy absorption can be adjusted with friction. The suture can be optimized using experiments and/or modeling, and in particular the failure modes of yielding and/or fracture of the tabs can be integrated in the models using solutions from frictional contact mechanics. The pullout mechanism of the materials presented here did not involve plastic deformations, but some of the designs fractured near the contact area. This type of failure, due to tensile stresses generated by the frictional shear tractions at the contact, can be delayed by lowering the coefficient of friction at the interfaces. A comprehensive study of a single jigsaw-like tab indeed showed that in terms of optimization it is preferable to choose low friction coefficient with high locking angles [40]. Incorporating a second material at the interface [6,7], in a way similar to proteins and polysaccharides at the interfaces of biological materials, would also be beneficial to the material performance [18,41]. The design concepts presented here can be extended to materials composed of interlocked tabs with more than two stable configurations, with the perspective of achieving strength and toughness beyond what is reported here. Moreover, while the designs explored here are essentially two-dimensional, materials with three-dimensional multi-stable interlocking features can also be explored using 3D printing techniques. This approach can be used to toughen glasses and ceramics, two groups of materials whose range of applicability is limited by their low toughness. The BIMs also promise interesting perspectives such as ease of repair, re-manufacturability or multi-functionalities such as adjustable filtering of fine particles where the shape and size of the stable positions can be tailored to switch between coarse and fine filtering positions [42].

Acknowledgments

References

[1] K. Mittal, The role of the interface in adhesion phenomena, Polym. Eng. Sci. 17 (7) (1977) 467–473.

[2] J.M. Challen, P.L.B. Oxley, Explanation of the different regimes of friction and wear using asperity deformation models, Wear 53 (2) (1979) 229–243.

[3] R. Raj, M.F. Ashby, On grain boundary sliding and diffusional creep, Metall. Trans. 2 (4) (1971) 1113–1127.

[4] A.G. Evans, F.W. Zok, The physics and mechanics of fibre-reinforced brittle matrix composites, J. Mater. Sci. 29 (15) (1994) 3857–3896.

[5] S. Khandelwal, et al., Adaptive mechanical properties of topologically interlocking material systems, Smart Mater. Struct. 24 (4) (2015) 045037.

[6] M. Mirkhalaf, A.K. Dastjerdi, F. Barthelat, Overcoming the brittleness of glass through bio-inspiration and micro-architecture, Nat. commun. (5) (2014) 3166.

[7] M. Mirkhalaf, F. Barthelat, A laser-engraved glass duplicating the structure, mechanics and performance of natural nacre, Bioinspiration Biomimetics 10 (2) (2015) 026005.

[8] A.V. Dyskin, et al., Fracture resistant structures based on topological interlocking with non-planar contacts, Adv. Energy Mater. 5 (3) (2003) 116–119.

[9] E. Lin, et al., 3D printed, bio-inspired prototypes and analytical models for structured suture interfaces with geometrically-tuned deformation and failure behavior, J. Mech. Phys. Solids 73 (2014) 166–182.

[10] M. Mirkhalaf, J. Tanguay, F. Barthelat, Carving 3D architectures within glass: Exploring new strategies to transform the mechanics and performance of materials, Extreme Mech Lett (2016).

[11] O. Bouaziz, Geometrically induced strain hardening, Scr. Mater. 68 (1) (2013) 28–30.

[12] L.S. Dimas, et al., Tough composites inspired by mineralized natural materials: computation, 3D printing, and testing, Adv. Funct. Mater. 23 (36) (2013) 4629–4638.

[13] M.B. Cohn, C.-J. Kim, A.P. Pisano, Self-Assembling electrical networks: An application of micromachining technology, 1991.

[14] Y. Li, C. Ortiz, M.C. Boyce, Stiffness and strength of suture joints in nature, Phys. Rev. E 84 (6) (2011) 062904.

[15] J.W.C. Dunlop, R. Weinkamer, P. Fratzl, Artful interfaces within biological materials, Mater. Today 14 (3) (2011) 70–78.

[16] E. Lin, et al., Tunability and enhancement of mechanical behavior with additively manufactured bio-inspired hierarchical suture interfaces, J. Mater. Res. 29 (17) (2014) 1867–1875.

[17] P. Fratzl, I. Burgert, H.S. Gupta, On the role of interface polymers for the mechanics of natural polymeric composites, Phys. Chem. Chem. Phys. 6 (24) (2004) 5575–5579.

[18] F. Barthelat, Z. Yin, M.J. Buehler, Structure and mechanics of interfaces in biological materials, Nat. Rev. Mater. 1 (2016) 16007.

[19] Q. Zhang, et al., Pattern transformation of heat-shrinkable polymer by three-dimensional (3D) printing technique, Sci. Rep. 5 (2015).

[20] D. Restrepo, N.D. Mankame, P.D. Zavattieri, Phase transforming cellular materials, Extreme Mech. Lett. 4 (2015) 52–60.

[21] A. Pirrera, et al., Multi-stable cylindrical lattices, J. Mech. Phys. Solids 61 (11) (2013) 2087–2107.

[22] J.L. Silverberg, et al., Origami structures with a critical transition to bistability arising from hidden degrees of freedom, Nat. Mater. 14 (4) (2015) 389–393.

[23] S. Li, K. Wang, Fluidic origami with embedded pressure dependent multi-stability: a plant inspired innovation, J. R. Soc. Interface 12 (111) (2015) 20150639.

[24] H. Yasuda, J. Yang, Reentrant Origami-based metamaterials with negative Poisson's ratio and bistability, Phys. Rev. Lett. 114 (18) (2015) 185502.

[25] T.C. Shyu, et al., A kirigami approach to engineering elasticity in nanocomposites through patterned defects, Nat. Mater. (2015).

[26] D. Yang, et al., Phase-transforming and switchable metamaterials, Extreme Mech. Lett. 6 (2016) 1–9.

[27] B. Florijn, C. Coulais, M. van Hecke, Programmable mechanical metamaterials, Phys. Rev. Lett. 113 (17) (2014) 175503.

[28] W. Hamouche, et al., Basic criteria to design and produce multistable shells, Meccanica (2016) 1–16.

[29] A.R. Studart, Additive manufacturing of biologically-inspired materials, Chem. Soc. Rev. 45 (2) (2016) 359–376.

[30] J.R. Tumbleston, et al., Continuous liquid interface production of 3D objects, Science 347 (6228) (2015) 1349–1352.

[31] K.L. Johnson, K.L. Johnson, Contact Mechanics, Cambridge University Press, 1987.

[32] American Society for Testing and Materials, Standard Test Method for Static and Kinetic Coefficients of Friction of Plastic Film and Sheeting, 1894.

[33] L.C. Brinson, One-dimensional constitutive behavior of shape memory alloys: thermomechanical derivation with non-constant material functions and redefined martensite internal variable, J. Intell. Mater. Syst. Struct. 4 (2) (1993) 229–242.

[34] S. Barinov, Work-of-fracture determination for brittle materials, J. Mater. Sci. Lett. 12 (9) (1993) 674–676.

[35] A. Evans, K. Faber, Toughening of ceramics by circumferential microcracking, J. Am. Ceram. Soc. 64 (7) (1981) 394–398.

[36] F. Barthelat, R. Rabiei, Toughness amplification in natural composites, J. Mech. Phys. Solids 59 (4) (2011) 829–840.

[37] American Society for Testing and Materials, Standard test method for measurement of fracture toughness, 2011.

[38] U.G. Wegst, et al., Bioinspired structural materials, Nat. Mater. (2014).

[39] R. Wang, et al., Deformation mechanisms in nacre, J. Mater. Res. 16 (09) (2001) 2485–2493.

[40] I. Malik, M. Mirkhalaf, F. Barthelat, Bio-inspired "Jigsaw"-like interlocking sutures: Modeling, optimization, 3D printing and testing, J. Mech. Phys. Solids (2016) (submitted for publication).

[41] F. Barthelat, Architectured materials in engineering and biology: fabrication, structure, mechanics and performance., Int. Mater. Rev. 60 (8) (2015) 413–430.

[42] Y. Brechet, J. Embury, Architectured materials: expanding materials space, Scr. Mater. 68 (1) (2013) 1–3.